Benchmarking of Neutral Beam Current Drive Codes as a Basis for the Integrated Modeling for ITER

T. Oikawa[1,2], J.M. Park[3], A.R. Polevoi[1], M. Schneider[4], G. Giruzzi[4], M. Murakami[3], K. Tani[5], A.C.C. Sips[6], C. Kessel[7], W. Houlberg[1], S. Konovalov[8], K. Hamamatsu[2], V. Basiuk[4], A. Pankin[9], D. McCune[7], R. Budny[7], Y-S. Na[10], I. Voitsekhovich[11], S. Suzuki[12], ITPA/Integrated Operation Scenario Group (the former Steady State Operation Group)

[1] ITER Organization, St Paul lez Durance, France

[2] Japan Atomic Energy Agency, Naka, Ibaraki, Japan

[3] Oak Ridge National Laboratory, Oak Ridge, Tennessee, USA

[4] Association Euratom-CEA, DSM/IRFM, CEA/Cadarache, Saint-Paul-Lez Durance, France

[5] Nihon Advanced Technology Inc.

[6] Max-Planck-Institut für Plasmaphysik, EURATOM-Assoziation, Garching, Germany

[7] Princeton Plasma Physics Laboratory, Princeton, NJ, USA

[8] Kurchatov Institute, Moscow, Russia,   [9] Lehigh University, Bethlehem, PA, USA

[10] Dept. Nuclear Engineering, Seoul National University, Seoul, Korea,

[11] Culham Science Centre, Abingdon, UK,   [12] Osaka University, Osaka, Japan

e-mail contact of main author: toshihiro.oikawa@iter.org

Abstract. This paper discusses the results of a benchmark study in which the predictions of numerical codes for neutral beam current drive and heating were compared using the parameters of the reference ITER steady state scenario, as a collaboration work of in the frame of the ITPA-SSO group. The models employed in the benchmarked codes for each physics related to NB heating and current drive, such as the beam model, beam stopping cross section, fast ion solver, orbit effects and electron shielding, are reviewed and examined through comparison.

1 Introduction

Neutral beam injection (NBI) is a robust method for heating and current drive (CD) because it does not depend on any resonance conditions or coupling conditions at the edge. High-energy neutral beam current drive (NBCD) was experimentally validated for central current drive in JT-60U [1], giving a further confidence in ITER predictions. These features make NBCD a dominant non-inductive current drive source in ITER [2]. However, discrepancy from theoretical predictions has been reported for an off-axis NBCD case in ASDEX-UG [3], where the off-axis NBCD capability could have a substantial impact on prospected ITER hybrid [4] and steady-state scenarios [5]. Recent progress in diagnostics, equilibrium solvers and analysis techniques enable rather detailed comparisons with NBCD codes. However, different codes give somewhat different results. Thus, we need to clarify physics implementations in NBCD codes, such as the beam model, ionization process, fast ion diffusion in the velocity space, orbit effects and electron shielding. Also from an integrated modeling viewpoint, an NBCD code benchmark is needed to establish a more solid basis for ITER operations.

2 The NB codes benchmarked

This NB code benchmark study were done with three orbit following Monte-Carlo (MC) codes OFMC [6], ONETWO [7]/NUBEAM [8] and NEMO/SPOT [9], and two Fokker-Planck (FP) codes ACCOME [10] and ASTRA [11].

OFMC : The MC code OFMC follows fast particle guiding center orbits in an arbitrary axisymmetric geometry. The fast ion source is calculated by the MC technique using the parallel beam model with a bi-gaussian intensity profile and Janev's [13] or Suzuki's [14] fitting formula for the beam stopping cross-section incorporating the multi-step ionization process.

ACCOME : Used is the same models for beam and ionization as OFMC. The fast ion source

profile is bounce-averaged. ACCOME adopts numerically derived eigenfunctions of the bounce-averaged, two-dimensional Fokker-Planck equation [15] and also incorporates the energy diffusion term [16] derived in a regime of particle energy larger than an initial injection energy.

ONETWO : The guiding center orbit following MC code NUBEAM is employed in the 1.5D transport code ONETWO as an NBI solver. A NBI is modeled with the size and shape of the ion source grid, the vertical and horizontal focal lengths and divergence and the height and width of the aperture. Electron impact ionization and beam atom excitation correction are evaluated with Ref. [17]. Ionizations by collisions with the ions are calculated with Ref. [18] and [19].

ASTRA : The NBI module adopts a 2D Fokker-Planck equation derived for a cylinder plasma [16]. The NBI tilting is approximated by injection parallel to the equatorial plane crossing the same innermost flux surface, with scaling the beam pass length to the real one. Janev's fitting formula for the multistep ionization [13] is used. Effects of finite orbit width and finite ion Larmour radius are considered in the fast ion source and orbit loss by the 'first orbit' approximation. The trapped particles are excluded in the current drive calculation.

NEMO/SPOT : The code consists of a fast ion source calculation module NEMO and a guiding center orbit following module SPOT. A NBI is modeled with a rectangular or circular beam source and the vertical and horizontal focal points. ADAS [20] is used for beam ionization, including excitation correction.

Physics implementations of the codes are summarized in table 1.

	OFMC	ACCOME	ONETWO/ NUBEAM	ASTRA	NEMO/SPOT
Beam model	parallel, gaussian, MC particles	←	focus, aperture, divergence, MC particles	effective inj. geometry	focus, divergence MC particles
Ionization cross section	Janev [13] Suzuki [14]	←	[17–19]	Janev [13]	ADAS [20]
Ionization on beam ions	no	no	yes	no	yes
Fast ion solver	MC	2D FP [15]	MC	2D FP [16]	MC
Finite orbit width effects	yes	no	yes	First orbit for birth	yes
Diff. in $E > E_B$	yes	Gaffey [16]	yes	yes	yes
FLR corrections	loss to wall	no	birth	birth	birth
Loss	First wall (FW)	no	FW	Separatrix	FW
Orbit loss	yes	no	yes	First orbit	yes
Ripple loss	yes	no	yes	First orbit	yes
CX loss	yes	no	yes	First orbit	no
Recapture of CX fast neutrals	yes	no	yes	no	no
Heating rates	yes	no	yes	yes	yes
Current source	yes	yes	yes	yes	yes
Particle sources	yes	yes	yes	yes	yes
Momentum sources	Collisional, CX loss	no	Collisional+$J \times B$+ Thermalization-CX loss	Birth	no
Rotation effects	yes	no	yes	no	no
Electron shielding model	Cordey [21], Start&Cordey [22]	←	Hirshman [23]	Kim [24]	Lin-Liu [25]

Table 1. The NBCD codes used in this benchmark and physics models included in the codes.

3 NBCD code benchmarking study

Plasma and NBI parameters

The magnetic flux surface geometry and kinetic profiles used in this benchmark are shown in Fig.1. The plasma parameters correspond to the reference ITER 'Scenario 4' (steady-state
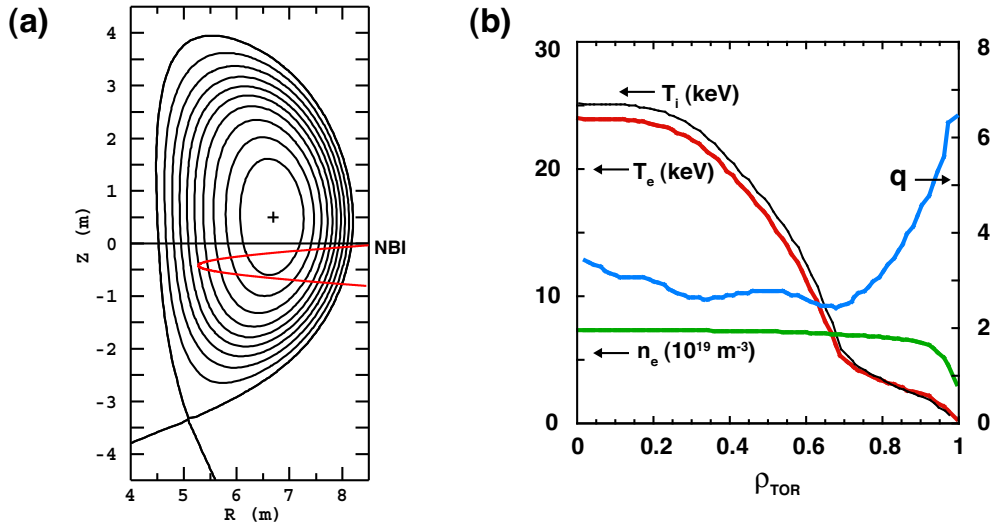
FIG. 1. The reference ITER Scenario 4 [26] : **(a)** *Equilibrium and the poloidal projection of the most off-axis NB injection.* **(b)** *The radial profiles of the temperatures, electron density and safety factor.*

Species	D^0	Launching point	(29955, 5295, 1343) mm
Beam energy E_B	1 MeV	Tangency radius R_{tang}	5295 mm ($Z@R_{\text{tang}}$ =-420 mm)
Injection power P_{NB}	33 MW	Injection angle	3.365 deg. (downward)
$E_B : E_B/2 : E_B/3$	$1 : 0 : 0$	$1/e$ radius of intensity	0.3 m (vert.), 0.2 m (hor.)@R_{tang}

Table 2. NBI parameters used in the benchmark (EDA2001).

at $Q = 5$) [26] with $R_0 = 6.35$ m, $a = 1.85$ m, $B_T = 5.3$ T, $I_p = 9$ MA, $< n_e >= 6.74 \times 10^{19}$ m^{-3}, $n_e(0) = 7.27 \times 10^{19}$ m^{-3}, $T_e(0) = 23.9$ keV and $T_i(0) = 25.2$ keV. Zero plasma rotation is assumed. The density ratio of the bulk deuterium and tritium is $1 : 1$. The benchmark condition different from the reference Scenario 4 is the impurity condition. Carbon is used as the single impurity species and helium is not considered. A constant profile of $Z_{\text{eff}} = 2.17$ is assumed.

The EDA2001 NBI design [27] is used in this study. The initial installation of the NB system consists of two injectors. Each injector will deliver a deuterium beam of 16.5 MW, with energy of 1 MeV. Within the NB duct height and heat load limitation, the beam can be aimed at two extreme positions (on-axis and off-axis) by tilting the beam source around a horizontal axis on its support flange. The most off-axis injection angle of 3.365 degree downward is used in the benchmark. The NBI parameters are summarized in table 2. It should be noted that the ion source location and tilting range has been changed in the latest 2007 ITER NBI design.

Results of the NBCD Code Benchmark

All the codes were run by using physics functions and models that are usually used, except the CX and ripple losses being turned off. OFMC, ACCOME and NUBEAM were run for the equilibrium file given in the EQDSK format. ASTRA and NEM/SPOT does not read an EQDSK file. ASTRA solves the current profile and the flux surfaces by itself without using the EQDSK file. NEMO/SPOT solves equilibrium for a separatrix and current density profile of the EQDSK file, resulting in a slightly different equilibrium with a smaller triangularity. In the MC codes OFMC, NUBEAM and NEMO/SPOT, the number of the Monte-Carlo particles is 30000, 5000 and 11000, and the criteria of the fast ion thermalization is $1.25T_i$(local), $1.5T_i$(local) and $2T_e$(axis), respectively. ACCOME uses 20000 MC particles in calculating the fast ion source. NUBEAM was run for a long enough time for reaching steady-state, and the profiles are averaged over 2.5 second, which is longer than the slowing down time.

Figure 2 shows a comparison of the fast ion source S_f, fast ion density n_f, powers to
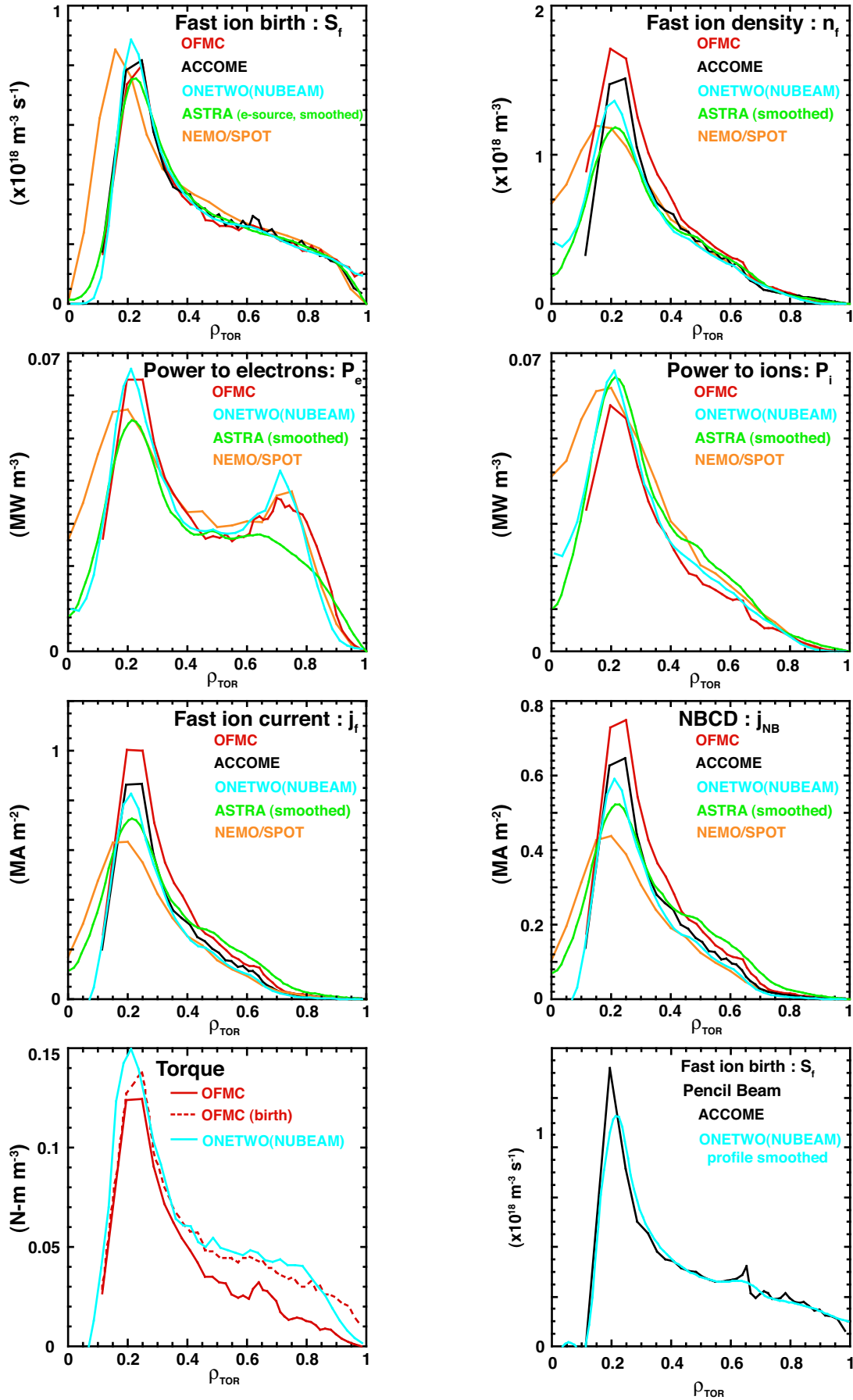
FIG. 2. Comparison of the fast ion source (electron source for ASTRA), fast ion density, fast ion current density, NB driven current density, powers deposited to electrons and ions (bulk+impurity) and torque computed by the codes. The ASTRA profiles and the NUBEAM pencil case are spatially smoothed, while the other profiles are unsmoothed.

electrons and ions(bulk+impurity) P_e, P_i, fast ion current density profile j_f, NB driven current density j_{NB} and torque input. Here the normalized minor radius defined with the toroidal flux ρ_{TOR} are used in the profiles in this paper. The S_f profile is calculated with including the multi-step process by the codes. OFMC and ACCOME evaluate S_f at the ionization point, while in NUBEAM and NEMO the fast ion guiding center is distributed over gyro-radius randomly. ASTRA distributes new born fast ion energy over the Larmour radius and the finite orbit width estimated by the 'first orbit' approximation. Here it should be noted that the ASTRA profile shown is the electron source. OFMC, ACCOME and NUBEAM give very similar fast ion birth profiles. NEMO gives a similar profile but with the peak location around $\rho \sim 0.2$ being shifted, which may be due to the different equilibrium. In order to separate the effects of the beam model and stopping cross-section carefully, birth profiles by ACCOME and NUBEAM are compared for a pencil beam injection of 1 cm radius in the bottom right plot of Fig. 2. It is found that Janev's fitting formula for beam stopping and the atomic data set used in NUBEAM gives nearly identical profiles. The difference in the peak value at $\rho \sim 0.2$ may be mostly explained with the smoothing in the NUBEAM case. The slight different peak location is due to a coarse surface grid near the magnetic axis in ACCOME (40 Ψ grids regularly spaced). From the birth profile comparisons for the two beam cases (the real beam and pencil beam), we can state that difference originating from the beam model is small in the present case. For testing the beam models, we need to compare them with an exact beam model reproducing all the beam line components of the ITER NBI system.

P_e and P_i by OFMC and NUBEAM generally agrees. However, slight but visible discrepancy is observed in spite of almost identical fast ion source profiles. OFMC, NUBEAM and SPOT shows a peak at $\rho \sim 0.7 - 0.8$ in P_e, while the ASTRA profile does not have such a peak. This can be partially explained with the orbit loss treatment in ASTRA. As in table 3, ASTRA gives 1.1 MW orbit loss, contrary to the zero value by the MC codes. ASTRA judges a new born fast ion is immediately lost if the first orbit crosses the separatrix, which is inappropriate unless the first wall is close to the separatrix. Figure 3 shows an ASTRA calculation without the 'orbit averaging'. Here the 'orbit averaging' in ASTRA does distributing a new born fast ion over the width of its first orbit, then ASTRA judges if each of the distributed fast ions is lost. In the case without 'orbit averaging' the orbit loss is reduced to 0.1 MW and the peripheral electron heating increases. This means that the number of the particles (numerical weight) having 'loss' orbits increases in the 'orbit averaging' case. The conclusion drawn is that the orbit loss judgement by crossing the separatrix gives an erroneous result, not that the 'first orbit' approximation is unsatisfactory.

In the j_f plot one can find $j_f(\text{OFMC}) > j_f(\text{ACCOME}) > j_f(\text{NUBEAM})$ in spite of $S_f(\text{OFMC}) \approx S_f(\text{ACCOME}) < S_f(\text{NUBEAM})$, leading to $20 - 30\%$ more total fast ion current I_f by OFMC (table 3). The same tendency is observed in n_f in the whole region. These may indicate a longer slow down time in OFMC. ACCOME also has a similar tendency but less than OFMC. In SPOT fast ions seem to suffer more pitch angle scattering than in NUBEAM. The difference between OFMC and ACCOME can be explained partially by the finite orbit width effect, where I_f by OFMC is reduced to 3.38 MA by omitting the vertical drift term in the guiding center orbit equation. Next we compare the two FP codes ACCOME and ASTRA, which employs a bounce-averaged and cylinder FP equations, respectively. ASTRA shows larger j_f in $\rho > 0.4$ than ACCOME, while n_f is nearly same. There are two possible explanations for this. (1) For the off-axis tilting beam injection in the present benchmark case, the ASTRA beam model of converting the real NBI geometry to a parallel injection geometry makes the pitch angle of new born fast ions more aligned to the local magnetic field at a flux surface. (2) Most fast ions are born in the low field side, and hence the bounce averaged parallel velocities of the

Code	I_f (MA)	I_{NB} (MA)	P_e (MW)	P_i (MW)	P_{loss} (MW)	
					Shinethrough	Orbit
OFMC	3.64	2.83	21.38	10.87	0.008	0.0
ACCOME	2.99	2.31	-	-	0.008	-
ONETWO(NUBEAM)	2.78	2.13	20.44	11.67	0.010	0.0
ASTRA	3.65	2.83	18.67	13.28	0.006	1.07
NEMO/SPOT	2.35	1.73	20.27	12.74 (11.16*)	0	0

Table 3. Integrated values from the codes for the fast ion currents, NBCD, powers to electrons and ions(bulk+impurity) and losses due to shinethrough and orbit. P_i of ASTRA and SPOT include the fast ion thermalization energy. *Subtracting from the ion heating the fast ion thermalization energy of $33 \, \text{MW} \times (2T_e(\text{axis})/E_B) = 1.58 \, \text{MW}$.
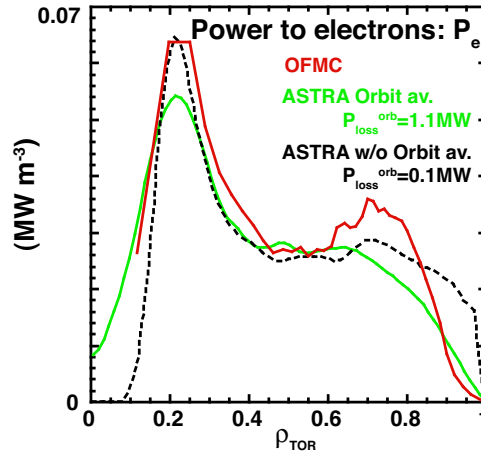

FIG. 3. ASTRA orbit averaging effect on P_e is shown.

beam ions are smaller than those at the birth locations.

The torque source is compared between OFMC and NUBEAM. OFMC considers only the collisional torque, while NUBEAM includes $J \times B$ torque due to the radial electric field induced by trapped particles' radial motion. However, there is a discussion if it is correct to fully count the trapped particle contribution [28].

The electron shielding represented by $\Gamma \equiv j_{NB}/j_f = 1 - F[1 - G]$ is compared in Fig. 4 (a), where F and G represent the fraction of electrons dragged along with the fast ions and the trapped electron correction, respectively. The models used in the codes are shown in table 1 and described in table 4. F is generally taken as Z_b/Z_{eff} (Z_b the fast ion charge), which is derived on the assumption that the electrons can be represented by a displaced Maxwellian, corresponding to the condition of the electron thermal velocity far greater than the fast ion velocity. OFMC and ACCOME adopt a result of the electron Fokker-Planck equation including these effects by Cordey et al [21], while the other codes use $F = Z_b/Z_{eff}$. Figure 4 (b) compares the Cordey model and $F = Z_b/Z_{eff} = 0.461$. The difference is less than 2 % inside a half minor radius and increases in the outer region ($\sim 10\%$ at $\rho_{TOR} = 0.9$). The trapped electron correction G is compared in Fig. 4 (c). OFMC and ACCOME use a numerical table of G provided by Start&Cordey [22] for plasmas in the banana regime with $Z_{eff} = 1 - 16$ and $\epsilon = 0.0 - 0.9$. Kim's formula [24] is in an excellent agreement with the Start&Cordey result. Lin-Liu's formula [25] is equivalent to Kim's one except rounding of numerical coefficients. In spite of this, a clear difference is observed between NEMO/SPOT (Lin-Liu), OFMC&ACCOME and ASTRA (Kim). This may result from the different equilibrium in NEMO/SPOT. The large deviation of the ONETWO result is observed in a low temperature regime of $\rho_{TOR} > 0.6$. This is because the NUBEAM model is applicable to all the regimes of the banana, plateau and Pfirsch-Schlüter, while the other models are derived in the banana regime.
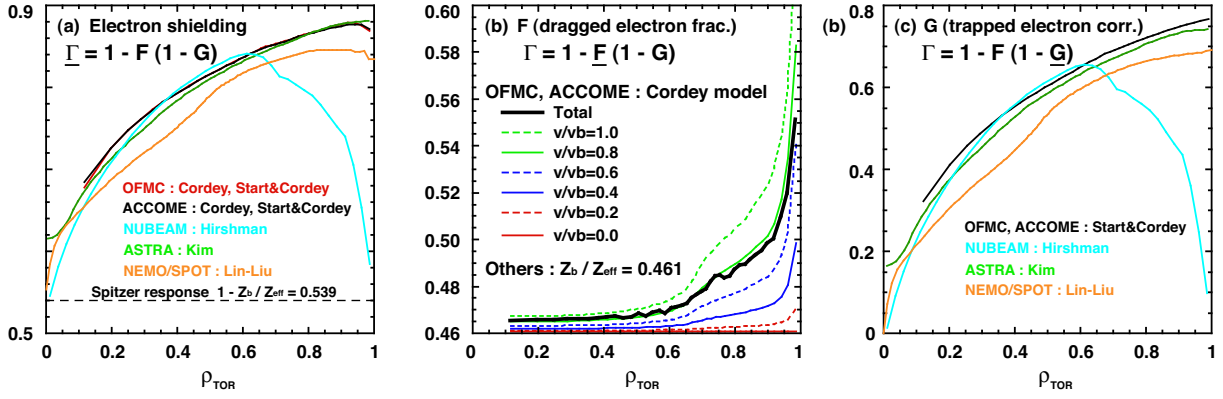
FIG. 4. Electron shielding models used in different codes. **(a)** *Electron shielding* Γ **(b)** *Electron response term F. The values for $v/v_b = 0.2, 0.4, 0.6, 0.8, 1.0$ and the total . ONETWO(NUBEAM), ASTRA and SPOT use $Z_b/Z_{eff} = 0.461$.* **(c)** *Trapped electron correction term G.*

Model	Applicability	F	G
Cordey [21]		$F(Z_{\text{eff}}, v_b/v_e^{\text{th}})$	
Start&Cordey [22]	$v_b/v_e^{\text{th}} = 0$ Banana regime		$G(Z_{\text{eff}}, \epsilon)$
Hirshman [23]	Banana, plateau, PS regimes	Z_b/Z_{eff}	$f_t \left[\dfrac{1.5Z_{\text{eff}}(K_{12}-2.5K_{11})+(1.414+3.25Z_{\text{eff}})K_{11}}{Z_{\text{eff}}(1.414+3.25Z_{\text{eff}})-2.25Z_{\text{eff}}^2} \right]$
Kim [24]	$v_b/v_e^{\text{th}} = 0$ Banana regime	Z_b/Z_{eff}	$\dfrac{x\left(0.75+2.21Z_{\text{eff}}+Z_{\text{eff}}^2\right)+x^2\left(0.35+1.24Z_{\text{eff}}+Z_{\text{eff}}^2\right)}{D^{\text{KM}}(Z_{\text{eff}},x)}$
Lin-Liu [25]	$v_b/v_e^{\text{th}} = 0$ Banana regime	Z_b/Z_{eff}	$\dfrac{x\left(0.754+2.21Z_{\text{eff}}+Z_{\text{eff}}^2\right)+x^2\left(0.348+1.243Z_{\text{eff}}+Z_{\text{eff}}^2\right)}{D^{\text{LL}}(Z_{\text{eff}},x)}$

Table 4. The electron shielding models used are applicable to arbitrary ϵ, where
$f_t \equiv 1 - (3/4)\langle B^2 \rangle \int_0^{1/B_{\max}} \lambda d\lambda / \langle (1-\lambda B)^{1/2} \rangle$, $x \equiv f_t/(1-f_t)$,
$D^{\text{KM}}(Z_{\text{eff}}, x) \equiv 1.41 Z_{\text{eff}} + Z_{\text{eff}}^2 + x \left(0.75 + 0.266 Z_{\text{eff}} + 2 Z_{\text{eff}}^2\right) + x^2 \left(0.35 + 1.24 Z_{\text{eff}} + Z_{\text{eff}}^2\right)$,
$D^{\text{LL}}(Z_{\text{eff}}, x) \equiv 1.414 Z_{\text{eff}} + Z_{\text{eff}}^2 + x \left(0.754 + 0.2657 Z_{\text{eff}} + 2 Z_{\text{eff}}^2\right) + x^2 \left(0.348 + 1.243 Z_{\text{eff}} + Z_{\text{eff}}^2\right)$
Fitting formulas for K_{11} and K_{12} in the banana, plateau and PS regimes are given by Hirshman [23].

4　Conclusions

An NBCD code benchmark has been done for the reference ITER steady state scenario with three orbit following Monte-Carlo codes and two Fokker-Planck codes.

· Difference in the fast ion source arising from different beam models is small for the ITER NBI parameters. However, necessary is a more detailed comparison with an exact beam model reproducing the complete beam line components.

· An agreement is observed in fast ion source profiles calculated with different beam stopping models including atomic excited states corrections.

· Heating profiles by the Monte-Carlo codes used generally agrees. More closely, however, visible differences are observed. The partitions to electrons and ions are different between OFMC and NUBEAM, while SPOT and NUBEAM give quite close partitions.

· The orbit loss judgment by if a fast ion crosses the separatrix causes an erroneous result.

· OFMC calculates larger fast ion density and fast ion current than NUBEAM, while SPOT gives smaller one than NUBEAM. Collision may be weaker in OFMC and more pitch angle scattering may occur in SPOT.

· Comparing the FP codes, ASTRA calculates larger j_f in $\rho > 0.4$ than ACCOME. This can be result from the non-bounce-averaged beam ion velocity and the simplified NBI geometry.

· The electron shielding models used agrees within 2 % in $\rho < 0.6$. In the peripheral, however, the models derived for the banana regime deviates from the NUBEAM model using Hirshman's coefficients applicable to the entire collisionality regime, although the total NBCD is almost

unaffected due to small fast ion current there.

This report was prepared as an account of work by or for the ITER Organization. The Members of the Organisation are the People's Republic of China, the European Atomic Energy Community, the Republic of India, Japan, the Republic of Korea, the Russian Federation, and the United States of America. The views and opinions expressed herein do not necessarily reflect those of the Members or any agency thereof. Dissemination of the information in this paper is governed by the applicable terms of the ITER Joint Implementation Agreement.

References

[1] OIKAWA, T., et al., Nucl. Fusion 40 (2000) 435; Nucl. Fusion 41 (2001) 1575.

[2] SHIMOMURA, Y., et al., PPCF 43 (2001) A385.

[3] HOBIRK, J., OIKAWA, T., et al., 30th EPS Conf. (2003) O-4.1B.

[4] KESSEL, C.E., et al., Nucl. Fusion 47 (2007) 1274

[5] GIRUZZI, G., et al., this conference, IT/P6-4.

[6] TANI, K., et al., Journal of Phys. Soc. Jpn. 50 (1981)1726.

[7] ST JOHN, H.E., et al., Proc. 15th Int. Conf. on Plasma Phys. and Control. Nucl. Fusion Research 1994, Seville, Spain, Vol. 3 (IAEA, Vienna, 1995) 603.

[8] PANKIN, A., et al., Comp. Phys. Comm. 159 (2004) 157.

[9] SCHNEIDER, M., et al., Plasma Physics and Controlled Fusion 47 (2005) 2087.

[10] TANI, K., AZUMI, M., DEVOTE, R. S., Journal of Computational Physics 98 (1992)332.

[11] PEREVERZEV, G., et al., IPP-Report IPP 5/98 (2002).

[12] POLEVOI, A. , SHIRAI, H. , TAKIZUKA, T. , JAERI Data/Code 97-014 (1997).

[13] JANEV, R.K., BOLEY, C.D. and POST, D.E., Nucl. Fusion 29 (1989) 2125.

[14] SUZUKI, S., et al., Plasma Physics and Controlled Fusion 40 (1998) 2097.

[15] CORDEY, J.G., Nucl. Fusion 16 (1976) 499.

[16] GAFFEY, J.D., J. Plasma Phys. 16 (1975) 149.

[17] JANEV, R.K., et al., Elementary Processes in Hydrogen-Helium Plasmas, Springer-Verlag, Berlin/New York, 1987.

[18] BARNETT, C.F., et al., Tech. Rep. ORNL-6086/V1, 1990.

[19] PHANEUF, R.A., JANEV, R.K., PINDZOLA, M.S., Tech. Rep. ORNL-6090/V5, 1987.

[20] ADAS SUMMERS, H.P., The ADAS User Manual, version 2.6 (2004), http://adas.phys.strath.ac.uk

[21] CORDEY, J.G., JONES, E.M. and START, D.F.H., Nucl. Fusion 19 (1979) 249.

[22] START, D.F.H. and CORDEY, J.G., Phys. Flulids 23 (1980) 1477.

[23] HIRSHMAN, S.P., Phys. Fluids 21 (1978) 1295.

[24] KIM, Y.B., CALLEN, J.D. and HAMNÉN, H., JET-R(88)02 (1988).

[25] LIN-LIU, Y.R. and HINTON, F.L., Phys. Plasmas 4 (1997) 4179.

[26] POLEVOI, A.R., et al., Proc. 19th IAEA Fusion Energy Conf. (2002) IAEA-CN-94/CT/P-08.

[27] ITER EDA Documentation Series No.24 *ITER Technical Basis*, IAEA, Vienna, 2002.

[28] TAKIZUKA, T., private communication.